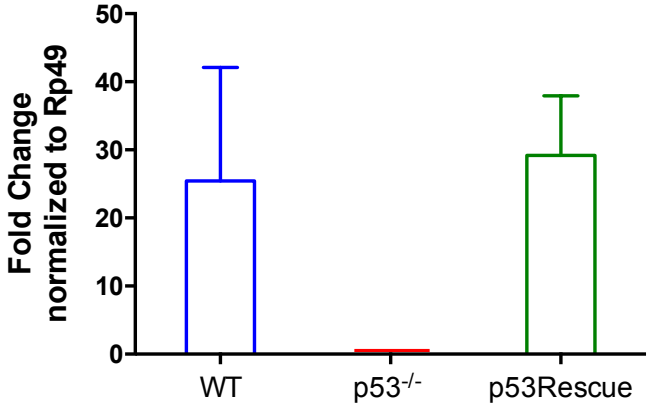

Supplemental Figure 1. p53 transcripts are expressed at similar levels in in WT and p53Rescue ovaries.

p53 transcript levels were measured by quantitative RT-PCR. WT and p53Rescue ovaries express p53 at similar levels. WT and p53Rescue samples are statistically significant from $p53^{-}$ samples were significantly different from WT (p value= 0.0287) and p53Rescue samples (p value =0.0167). Error bars represent standard deviations. See supplemental Table 6 for primer sequences (dp53_qPCR Fwd and Rev).

A

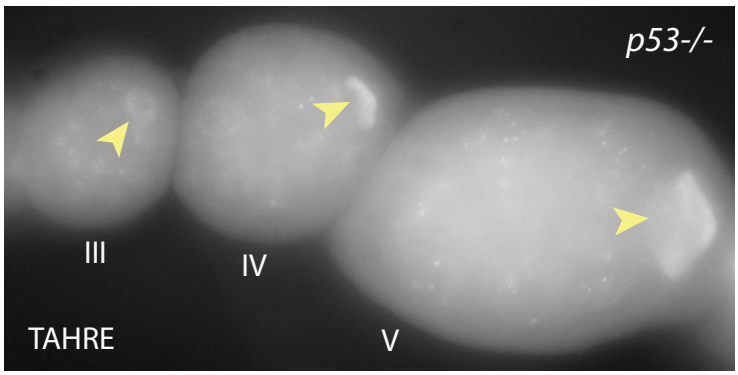

B

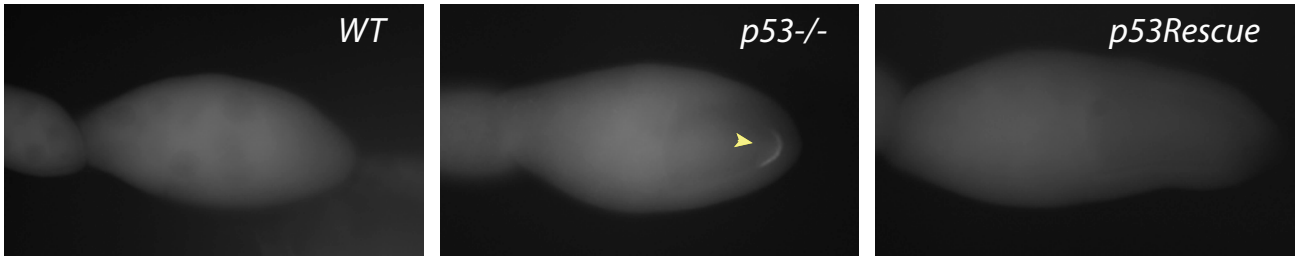

Supplemental Figure 2. TAHRE transcripts detected by FISH are first detected in the third egg chamber of p53^{-} animals

(A) The image shown is an example of fluorescent *in situ* hybridization (FISH) for TAHRE transcripts in the p53^{-} ovary to illustrate signal in different staged egg chambers. Images were scored as outlined in Supplemental Table 1. If transcripts are observed in the third egg chamber (III), the subsequent later egg chambers (IV, V) also have TAHRE signal (yellow arrows). The TAHRE FISH signal quantification is displayed in Supplemental Table 1 (below).

(B) These panels show TAHRE FISH in late stage egg chambers in WT, p53^{-} and p53Rescue strains. As quantified in Supplemental Table 1 (below), TAHRE expression in late stage egg chambers is readily detectable in the oocyte germ plasm of p53^{-} animals but not WT or p53Rescue strains.

Stage	WT			$p53^{-/-}$			p53Rescue		
	Number with TAHRE signal	Total (n=)	Percent (%)	Number with TAHRE signal	Total (n=)	Percent (%)	Number with TAHRE signal	Total (n=)	Percent (%)
Germ	0	60	0	0	93	0	0	45	0
I	0	60	0	0	93	0	0	45	0
II	0	60	0	0	93	0	0	45	0
III	0	60	0	15	93	15.1	0	45	0
IV	0	60	0	62	89	69.7	0	45	0
V	0	50	0	63	84	75	0	42	0
VI	3	72	4.2	54	62	87.1	4	36	11.1
VII	3	37	8.10	32	32	100	5	32	15.6

Supplemental Table 1. Stage Specific quantification of TAHRE FISH signal in WT, $p53^{-}$, and p53Rescue ovaries

The table indicates the number of ovaries with TAHRE signal, the total number assayed, and the percent positive for TAHRE signal in each stage of the ovariole. Genotypes are also indicated. Note that TAHRE signal is readily detected in $p53^{-}$ ovaries but rarely seen in WT or p53Rescue flies.

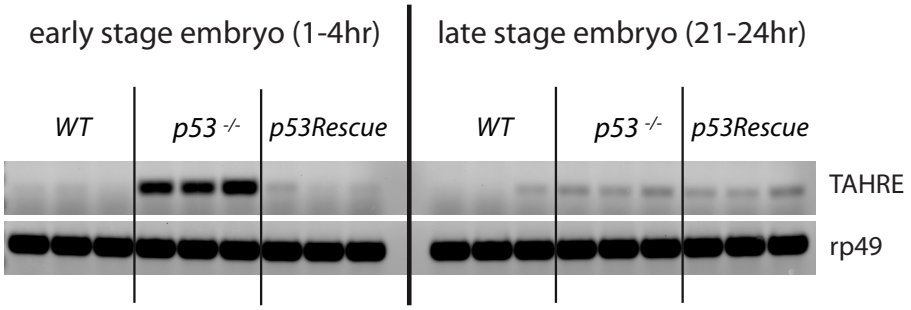

Supplemental Figure 3. TAHRE dysregulation is observed in early stage $p53^{-}$ embryos

TAHRE transcripts, measured by RT-PCR, are derepressed in the early 1-4hr old $p53^{-}$ embryo (left) when compared to WT and p53Rescue embryos. TAHRE dysregulation is not observed in late stage 21-24hr old embryos (right). The control reference transcript, rp49, is present at similar levels among all genotypes. Three independent biological replicates are shown for all genotypes.

Genotype	Trial	Infertile (n=)	Total (n=)	Percent Infertile (%)
$p53^{-/-}$	1	15	129	11.6%
	2	16	164	9.8%
	Total	**31**	**293**	**10.6%**
p53Rescue; $p53^{-/-}$	1	7	152	4.6%
	2	12	207	5.8%
	Total	**19**	**359**	**5.3%**

Supplemental Table 2. Elevated rates of infertility occur in $p53^{-/-}$ flies

The fertility of $p53^{-}$ and p53Rescue females were assessed by single pair matings to *yw* males (see methods). To negate background influences, $p53^{-}$ and p53Rescue flies were backcrossed into the *yw* background ($p53^{-/-}$ 17 generations; p53Rescue 10 generations) before testing fertility. The table indicates number of infertile animals, the total number assayed, and the percent infertile. A modest but reproducible increase in congenital sterility was observed in the $p53^{-}$ genotype compared to controls. $p53^{-}$ infertility is significantly different from the p53Rescue (* p value =0.0381) when using an unpaired t-test at the 95% confidence level (see methods).

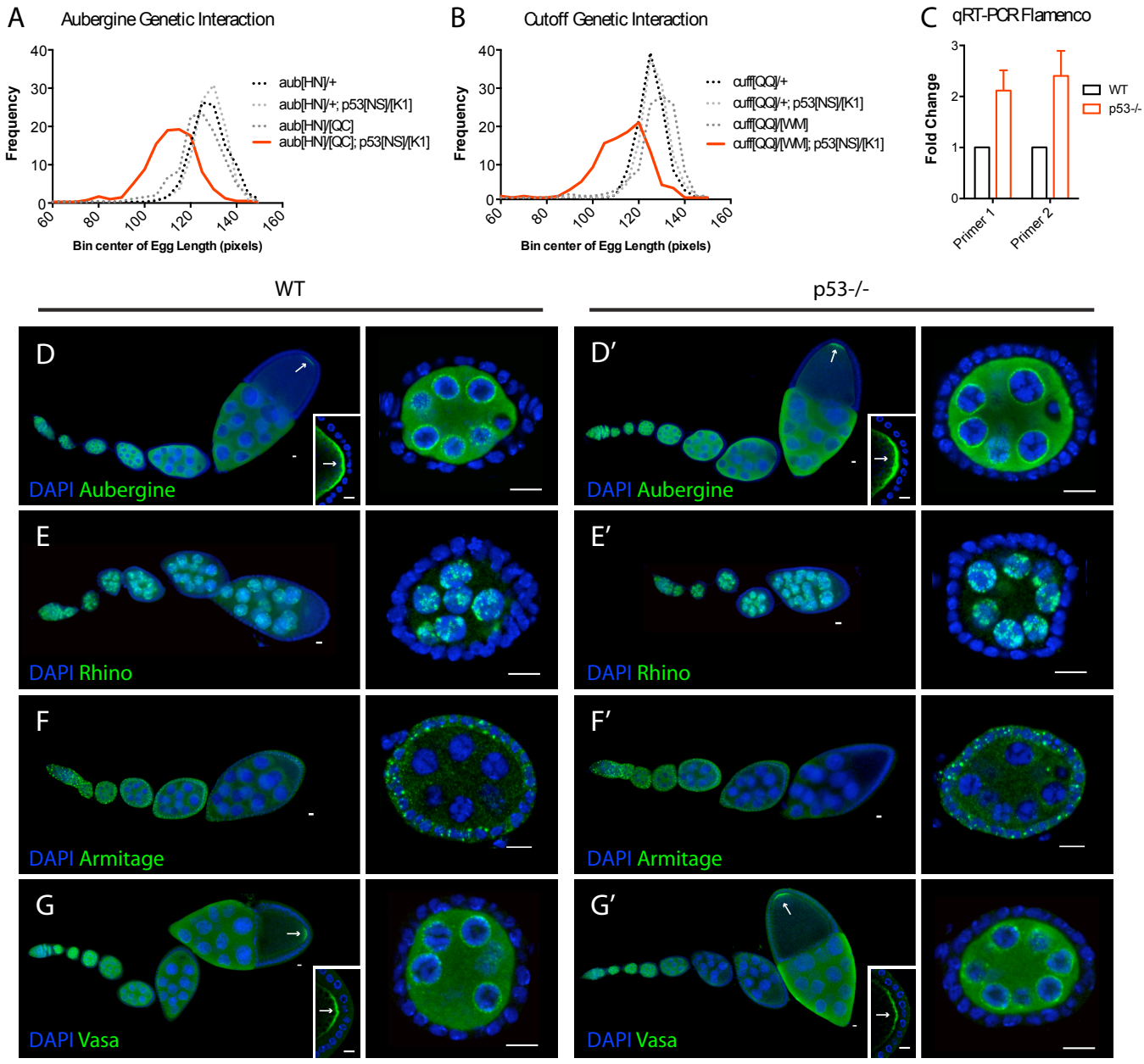

Supplemental Figure 4. p53 interacts with the piRNA network

(A-B) illustrate genetic interactions between p53 and the piRNA effectors, *aubergine (aub)* **(A)** *and cutoff (cuff)* **(B)**, detected here using egg morphology as a maternal effect readout (see methods). Eggs are generally normal in single mutants (dotted grey lines), but in *aub*$^{-}$*;p53*$^{-}$ or *cuff*$^{-}$*;p53*$^{-}$ double mutants (red line) severely stunted eggs are produced. **(C)** The piRNA precursor transcript, *Flamenco*, is significantly elevated in p53^{-} ovaries (red) compared to wild type (wt) controls (black). A similar phenotype is has previously been documented for piRNA pathway mutants where piRNA biogenesis is affected (Haase, et al. 2010; Vagin, et al. 2013). Data represent quantitative RT-PCR

assays, using non-overlapping primer pairs specific for this primary piRNA, as in (Vagin, et al. 2013).

(D-G') We performed immunohistochemistry (IHC) for several piRNA pathway proteins in WT and p53^{-} ovaries. As seen here, *Aubergine* **(D, D')**, *Rhino* **(E, E')**, *Armitage* **(F, F')** and *Vasa* **(G, G')** were normally localized and expressed at comparable levels in WT **(D, E, F, G)** and p53^{-} **(D', E', F', G')** animals. Higher magnification images of an egg chamber are shown in panels to the right. Smaller insets in **(D, D', G and G')** are posterior regions of later egg chambers highlighting germ plasm localization of *Aubergine* and *Vasa* (Kirino, et al. 2010). Scale bar 10μm

Antibodies used: α-aubergine and α-armitage were gifts from Mikiko Siomi (Nishida, et al. 2007; Saito, et al. 2010), α-rhino was gift from William Theurkauf (Klattenhoff, et al. 2009).

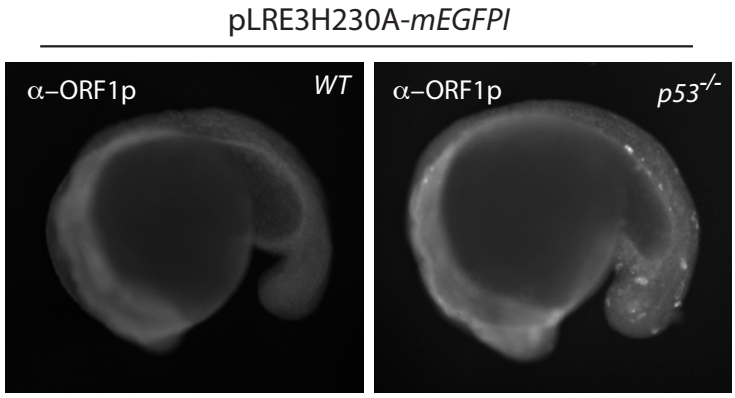

Supplemental Figure 5. Supporting data for Figure 3B.

Human L1 ORF1p (Rodic, et al. 2014) expression in 18 hour post-fertilization embryos injected with the control pLRE3H230A-*mEGFPI* expression construct (Coufal, et al. 2011). With this control, no integrations occur because the mutant pLRE3H230A-*mEGFPI* reporter lacks functional ORF2. Consistent with this, the reporter failed to produce EGFP^{+} cells in both WT and p53^{-} zebrafish (Supplemental Table 3). Furthermore, like its normal counterpart (Figure 3B) ORF1p, expressed from this control construct is abundant in p53^{-} embryos (right panel) but undetectable in parental wt embryos (left panel). Therefore, unlike integration events, derepression of ORF1p in p53 mutants is unaffected by mutations in ORF2. These data suggest that p53 restraint on retroelements, acts upstream of the integration event.

	Plasmid	EGFP+ (n=)	Total (n=)	Percent EGFP+ (%)
Injections into WT embryos				
	pLRE3-*mEGFPI* TR1	28	58	48.3%
	pLRE3-*mEGFPI* TR2	27	48	56.2%
	pLRE3-*mEGFPI* TR3	14	27	51.8%
	pLRE3-*mEGFPI* TR4	25	32	68.7%
	pLRE3H230A-*mEGFPI* TR1	0	30	0%
	pLRE3H230A-*mEGFPI* TR2	0	119	0%
	Uninjected control TR1	0	51	0%
	Uninjected control TR2	0	37	0%
	Uninjected control TR3	0	121	0%
Injections into $p53^{-/-}$ embryos				
	pLRE3-*mEGFPI* TR1	59	96	61.4%
	pLRE3-*mEGFPI* TR2	64	106	60.3%
	pLRE3-*mEGFPI* TR3	20	33	60.6%
	pLRE3H230A-*mEGFPI* TR1	0	49	0%
	Uninjected control TR1	0	9	0%
	Uninjected control TR2	0	37	0%
	Uninjected control TR3	0	132	0%

Supplemental Table 3. Quantification of LINE-1 reporter integration in WT and $p53^{-/-}$ zebrafish

The table quantifies the number of EGFP positive cells in parental wt and $p53^{-}$ zebrafish embryos injected with a LINE-1 movement reporter (pLRE3-*mEGFPI*). Different trials are designated as (TR1, etc). The number of $EGFP^{+}$ embryos, the total number of embryos, and the percent $EGFP^{+}$ embryos are indicated. The number of $EGFP^{+}$ embryos include both class I and class II embryos. The number of EGFP+ cells per embryo are graphed in Figure 3C'. Note that $EGFP^{+}$ cells were never observed with uninjected control animals or with a mutated version of the reporter (pLRE3H230A-*mEGFPI*).

Genotype	Trial	Unfertilized (n=)	Total (n=)	Percent Infertile (%)
$p53^{-/-}$	1	135	491	27.5%
	2	82	255	32.1%
	3	82	247	33.3
	Total	**299**	**993**	**30.1%**
WT(AB)	1	130	1108	11.7%
	2	10	243	4.1%
	3	41	576	7.1
	Total	**181**	**1927**	**9.4%**

Supplemental Table 4. Elevated rates of infertility occur in $p53^{-}$ zebrafish

The fertility of $p53^{-}$ and WT zebrafish was assessed by scoring the number of unfertilized eggs after matings (see methods). The table indicates number of unfertilized embryos, the total number assayed, and the percent unfertilized. We observed a consistent three fold increase in the number of unfertilized embryos in the $p53^{-}$ fish when compared to the WT. $p53^{-}$ infertility is significantly different from the WT (* p value =0.0012) when using an unpaired t-test at the 99% confidence level (see methods).

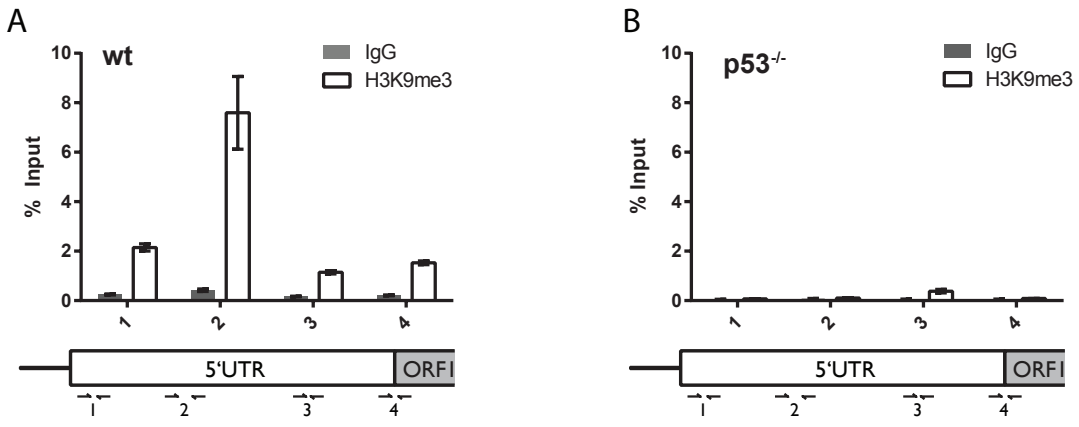

-

Supplemental Figure 6. ChIP Biological Replicate displays similar pattern of H3K9me3 levels across the L1 5' UTR

(a,b) H3K9 trimethylation across the synthetic LRE3 retroelement 5' UTR in wild type (a) and p53^{-} (b) zebrafish. Second biological replicate for ChIP analysis performed in 4 hpf wild type zebrafish injected with the LRE3 reporter construct using a H3K9me3 antibody (open bars) and control IgG (closed bars). H3K9 trimethylation levels were determined at four sites (1-4) spanning the L1 5' UTR by droplet digital PCR (see schematic, bottom panel). H3K9 trimetylation levels were normalized to input. 95% confidence intervals are indicated.

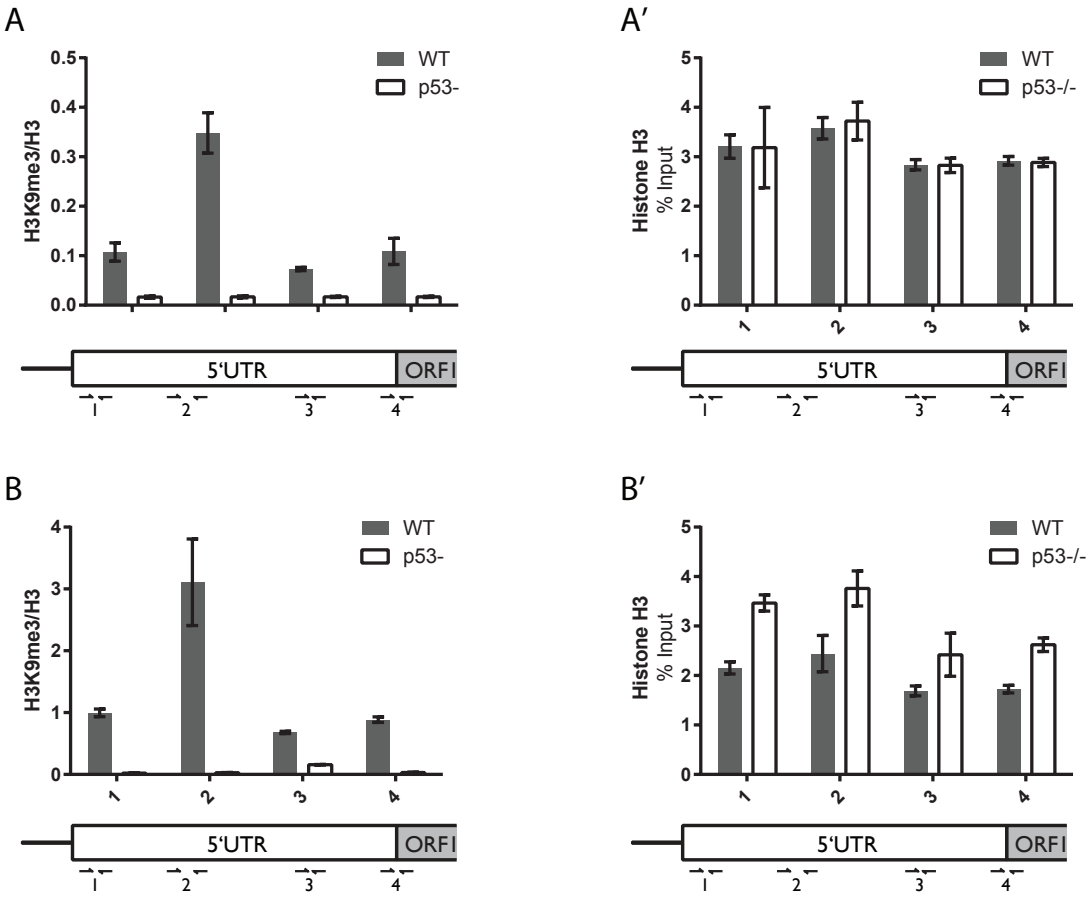

Supplemental Figure 7. Histone H3K9me3 and total H3 levels across the L1 5' UTR

(A) H3K9me3 calculated as a percentage of total H3 is presented for both WT (grey bars) and $p53^{-/-}$ (open bars) genotypes. 95% confidence intervals are indicated. (A') Total H3 levels across the L1 5' UTR normalized to input for wt (grey bars) and $p53^{-/-}$ (open bars). 95% confidence intervals are indicated. (A',B') A second biological replicate indicating H3K9me3 levels normalized to total H3 (B) and H3 normalized to input (B'). 95% confidence intervals are indicated. Note that H3K9me3 enrichment peaks at primer 2 in wt fish (grey bars), but is largely absent in $p53^{-/-}$ animals (open bars) in both biological replicates (compare (A) and (B)).

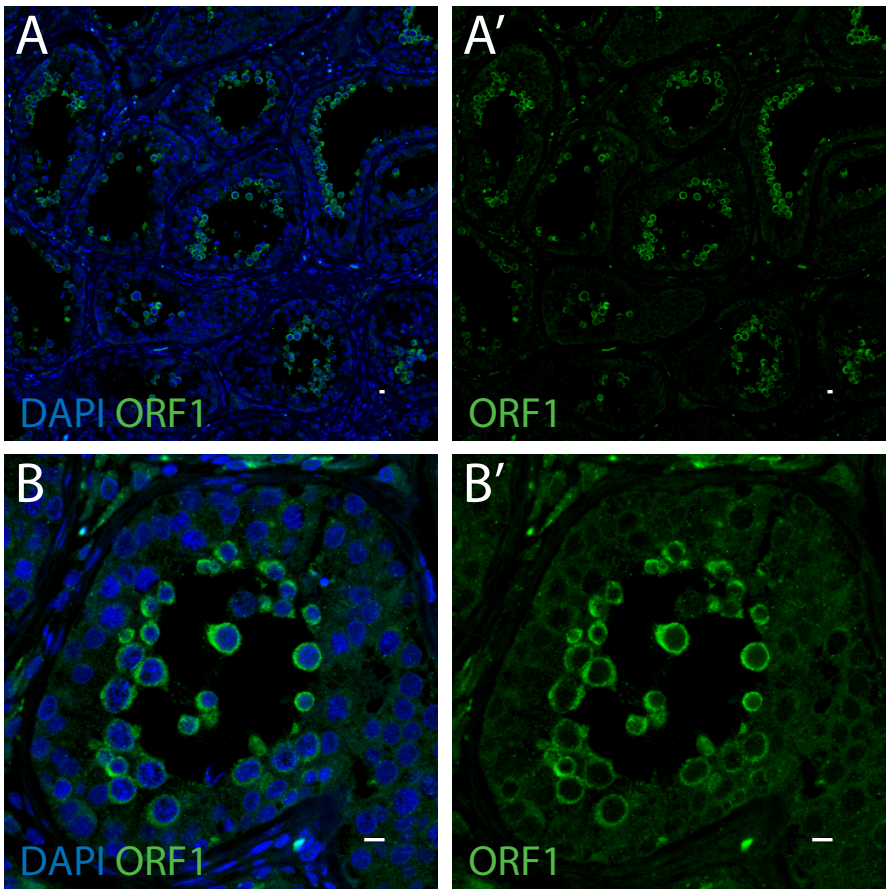

Supplemental Figure 8. LINE-1 ORF1p expression in human testis

Validation of the human LINE-1 ORF1p antibody (Rodic, et al. 2014) by detecting ORF1p expression (green) in human testis. (A-A') are low magnification images of seminiferous tubules. (B-B') are high magnification images of a single seminiferous tubule. Robust ORF1p expression (green) is observed in the human male germline as previously reported (Ergun, et al. 2004). (A' and B') are the same images as shown in (A and B, respectively) but without DAPI counterstain (blue) to better appreciate ORF1p expression.

CMC 11

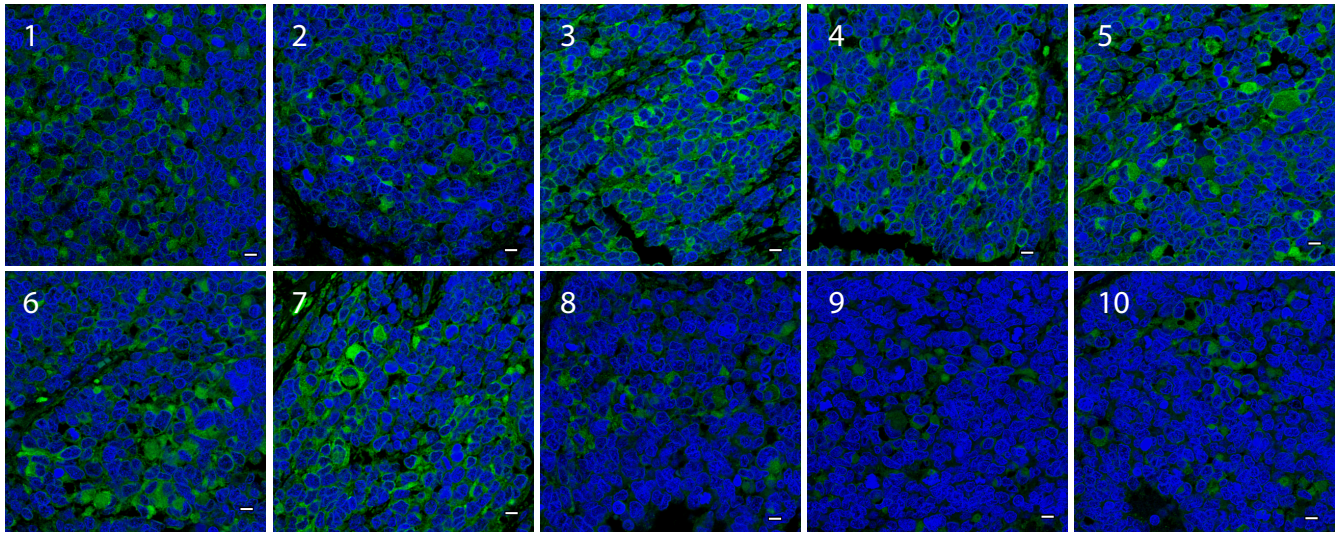

CMC 23

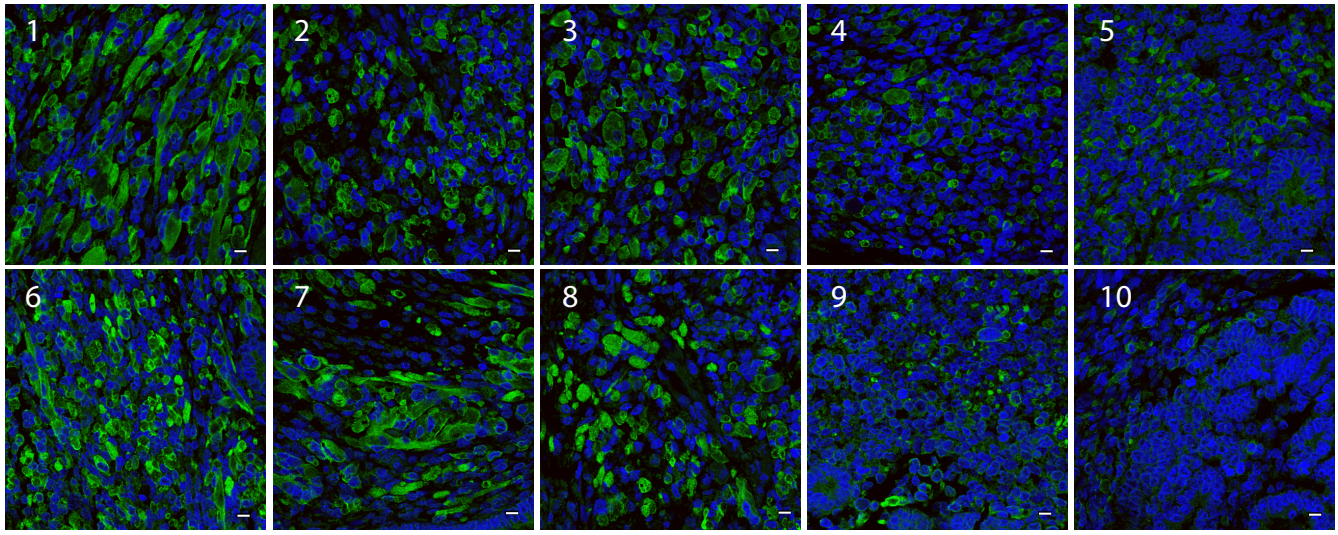

CMC 59

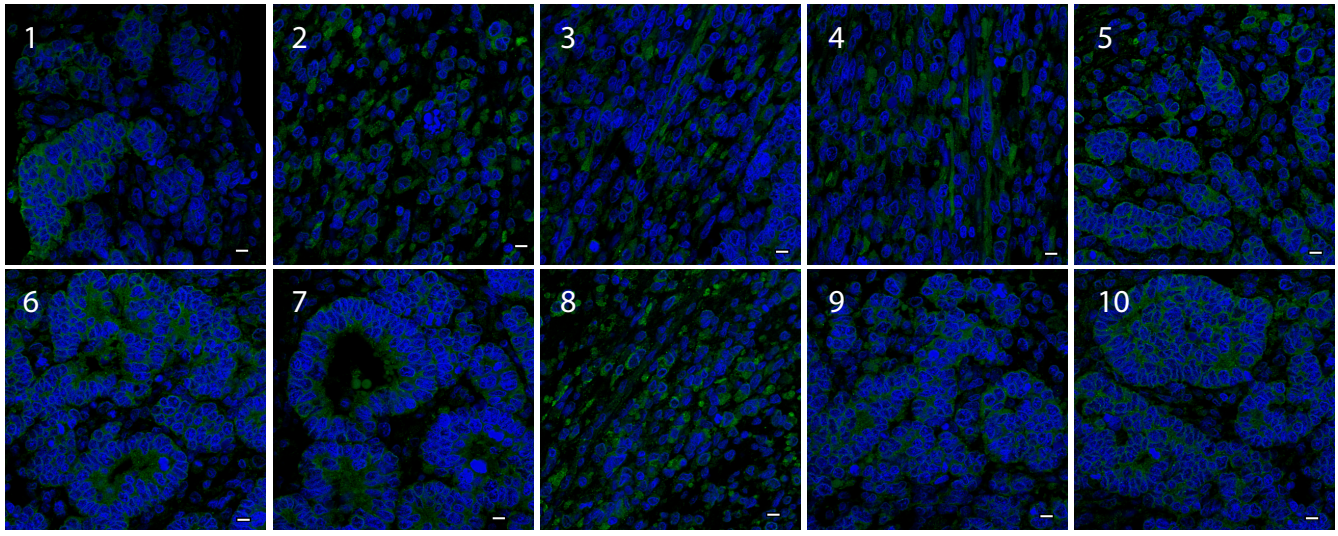

CMC 12

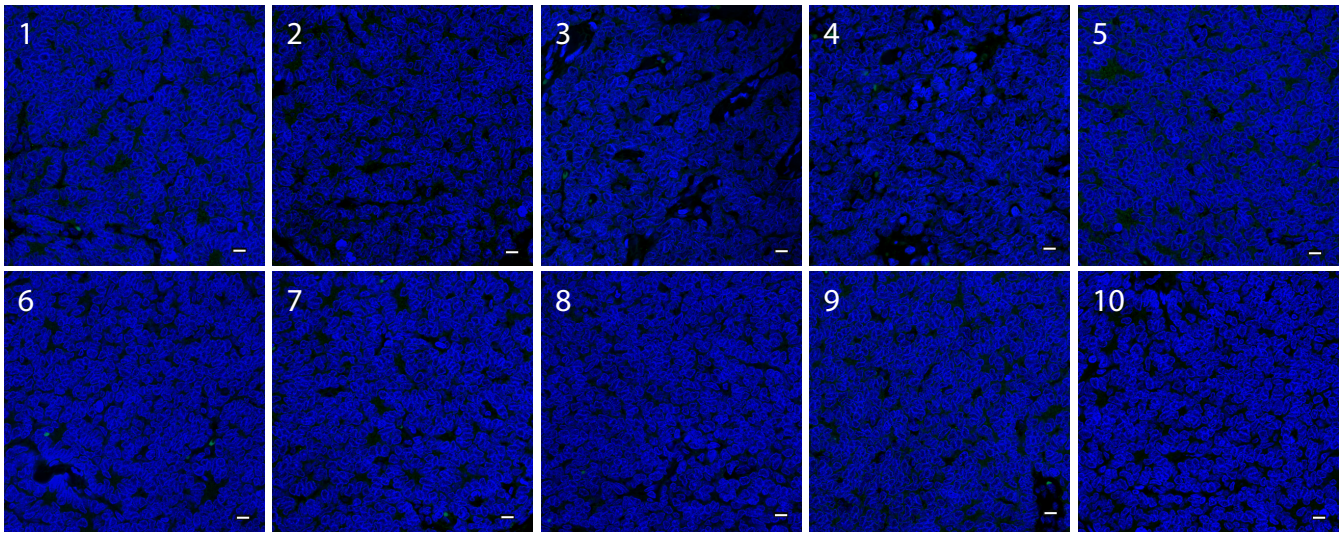

CMC 16

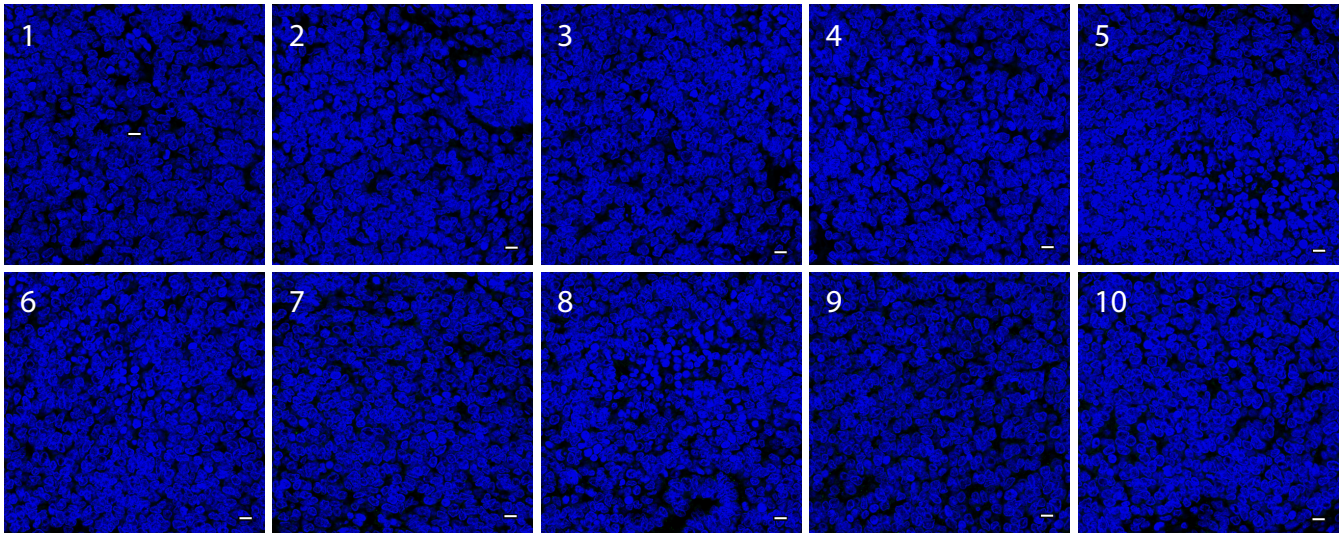

CMC 17

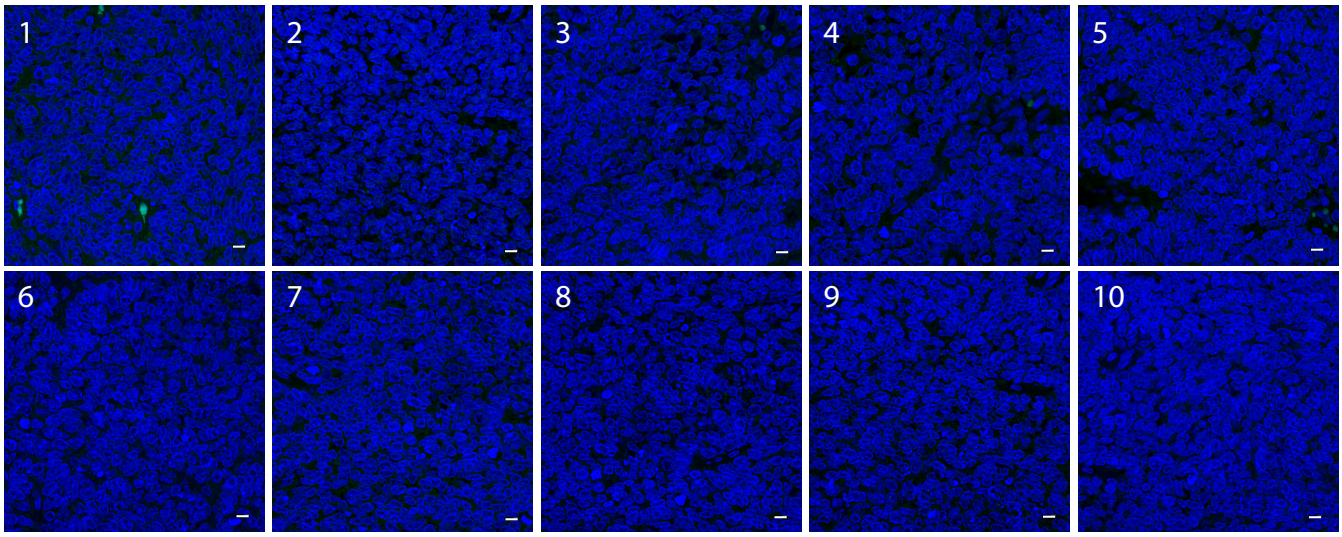

Supplemental Figure 9. Wilms Tumor Supporting Data

Wilms tumors were stained for human LINE-1 ORF1p (Rodic, et al. 2014) (green) and counterstained with DAPI (blue). Shown here are ten random fields of view taken for tumors that are wt for p53 (85, 87, 89) or mutant for p53 (11, 23, 59). Tumors that are mutant for p53 (11, 23, 59) show dramatically elevated LINE-1 ORF1p expression within all 10 fields of view. The normalized fluorescence intensity (see methods) for each field of view is graphed in Figure 5A'. Scale bars, 10μm.

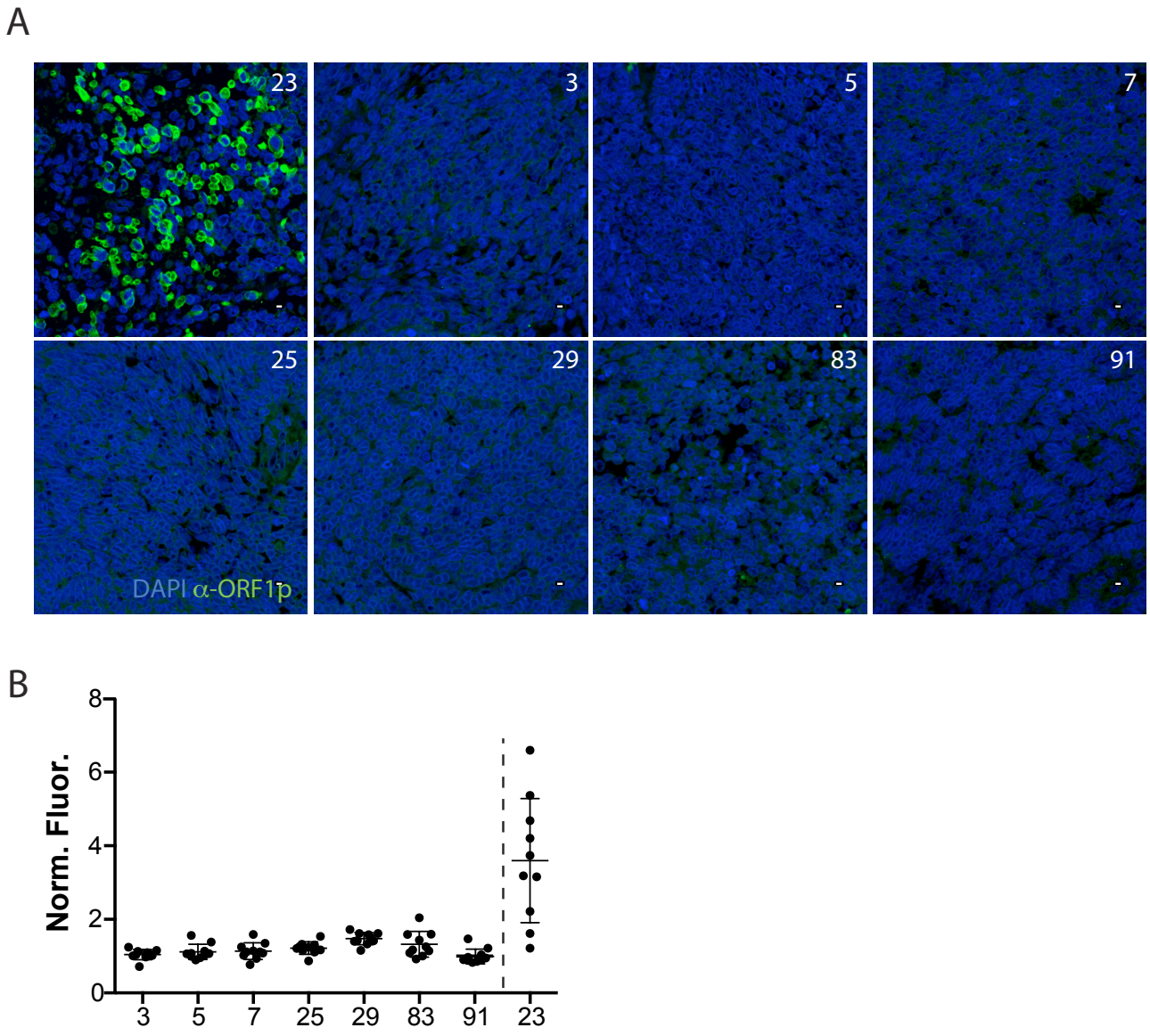

Supplemental Figure 10. Additional Wilms Tumor Data

(A) Wilms tumors were stained for human LINE-1 ORF1p (Rodic, et al. 2014) (green) and counterstained with DAPI (blue). Shown here are representative fields of view for tumors that are wt for p53 (3, 5, 7, 25, 29, 83, 91) or mutant for p53 (23). The tumor mutant for p53 (23) is used as a positive control here and was previously used in studies shown in Figure 5A and Supplemental Figure 10. The tumor mutant for p53 (23, top left panel in A) shows dramatically elevated LINE-1 ORF1p expression and the seven additional tumors that are wt for p53 (3, 5, 7, 25, 29, 83, 91). The normalized fluorescence intensity (see methods) for ten fields of view per tumor is graphed in Figure **(B)**. Scale bars, 10μm.

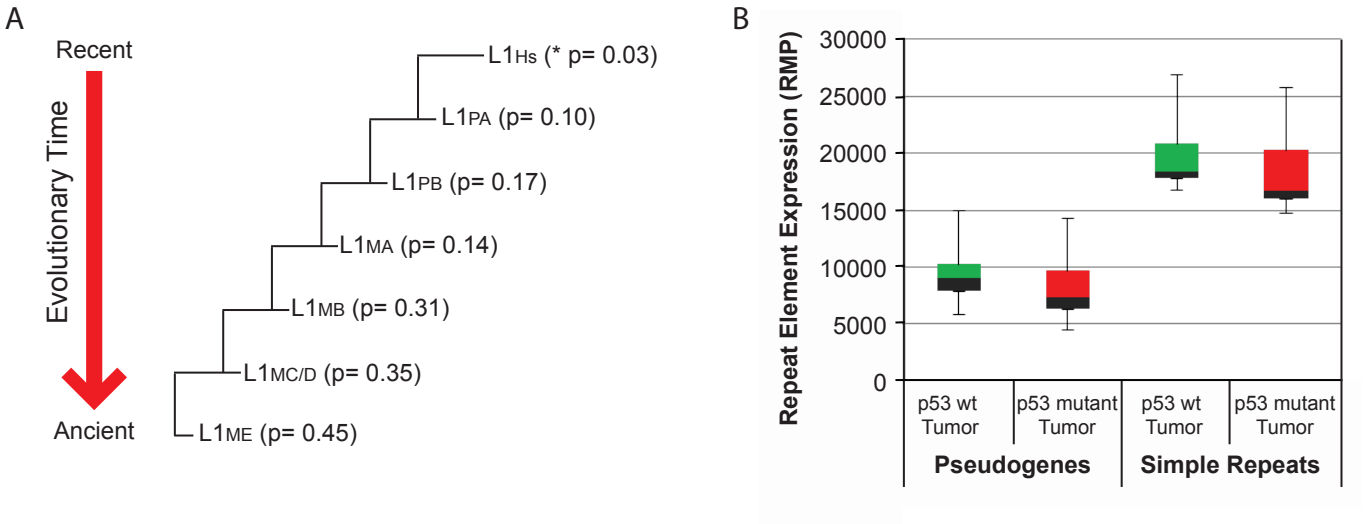

Supplemental Figure 11. Links between mutant p53 and elevated LINE-1 activity are specific and degrade over evolutionary distance. Support for Figure 6.

(A) The evolutionary phylogeny of LINE-1 elements lineages (Giordano, et al. 2007; Khan, et al. 2006) is schematized with p values for correlations to p53 status. As shown in Figure 6, RNA seq data was interrogated from eighteen colon cancer patients (8 wt and 10 p53 mutant) for dysregulated LINE-1 activity. Statistically significant differences in LINE-1 lineage expression levels in p53 wild type and p53 mutant samples were determined by Mann Whitney U test. Cancers bearing p53 mutations are significantly elevated for $L1_{HS}$ activity relative to cancers that are wild type for p53 (* p value= 0.03). Note that the $L1_{HS}$ subfamily includes full-length, human specific L1 elements. The $L1_{M}$ lineage ($L1M_{A-E}$) is comprised of L1 retroelements found across mammals, the $L1_{P}$ lineage ($L1_{PA}$ and $L1_{PB}$) of L1 retroelements is found across primates. Expression values for each lineage were calculated by summing RPM normalized read counts for each lineage member. Note that as evolutionary distances increase, p-values for correlations to p53 mutant status also increase.

(B) Pseudogenes and simple repeat expression data serve as controls for data in Figure 6. As in Figure 6, the x axis indicates the repeat element and p53 genotype of the colon cancers profiled (8 wt and 10 p53 mutant). The Y axis indicates repeat element expression in reads per million (RPM). Tops of boxes are 75th percentile. Bottoms of boxes are 25th percentile. Medians are at box intersections. Upper and lower whiskers are maximum and minimum values respectively. No statistically significant differences in the expression of pseudogenes (p-value=0.30772) or simple repeats (p-value=0.19706) for p53 WT (green) and p53 mutant (red) genotypes are seen. In

contrast, cancers bearing p53 mutations are significantly elevated for $L1_{HS}$ activity relative to cancers that are wild type for p53 (* p value= 0.03) (Figure 6).

Wilms		Colon Cancer	
Sample ID	**TP53**	**Sample ID**	**TP53**
3	WT	TCGA-A6-2671	V173/ Frameshift
5	WT	TCGA-A6-2678	R196*/R248Q
7	WT	TCGA-A6-2679	WT
11	V274L	TCGA-A6-2680	R196*/S241
23	R158H	TCGA-A6-2682	T125M/C176W
25	WT	TCGA-A6-2683	R175H
29	WT	TCGA-A6-2684	V173L
59	R342P	TCGA-A6-2685	WT
83	WT	TCGA-AA-3514	WT
85	WT	TCGA-AA-3516	WT
87	WT	TCGA-AA-3517	Q331H
89	WT	TCGA-AA-3518	WT
91	WT	TCGA-AA-3520	D207N
		TCGA-AA-3522	WT
		TCGA-AA-3525	WT
		TCGA-AA-3527	WT
		TCGA-AA-3531	C238Y
		TCGA-AA-3534	K164R/R213R

Supplemental Table 5. P53 mutations in Wilms tumors and Colon cancers

Summary of TP53 mutations in Wilms (left) and Colon Cancer (right) patients. TP53 mutations in Wilms tumors were previously reported in (Rakheja, et al. 2014). TP53 mutations are classified as missense, nonsense, or deletions. Nonsense mutations are indicated by *. All p53 mutant Colon Cancer samples contain a pathogenic amino acid substitution, based on classifications curated at theTP53 database (Petitjean, et al. 2007). Note, all matched normal tissue for the colon cancer data set were WT for TP53.

.

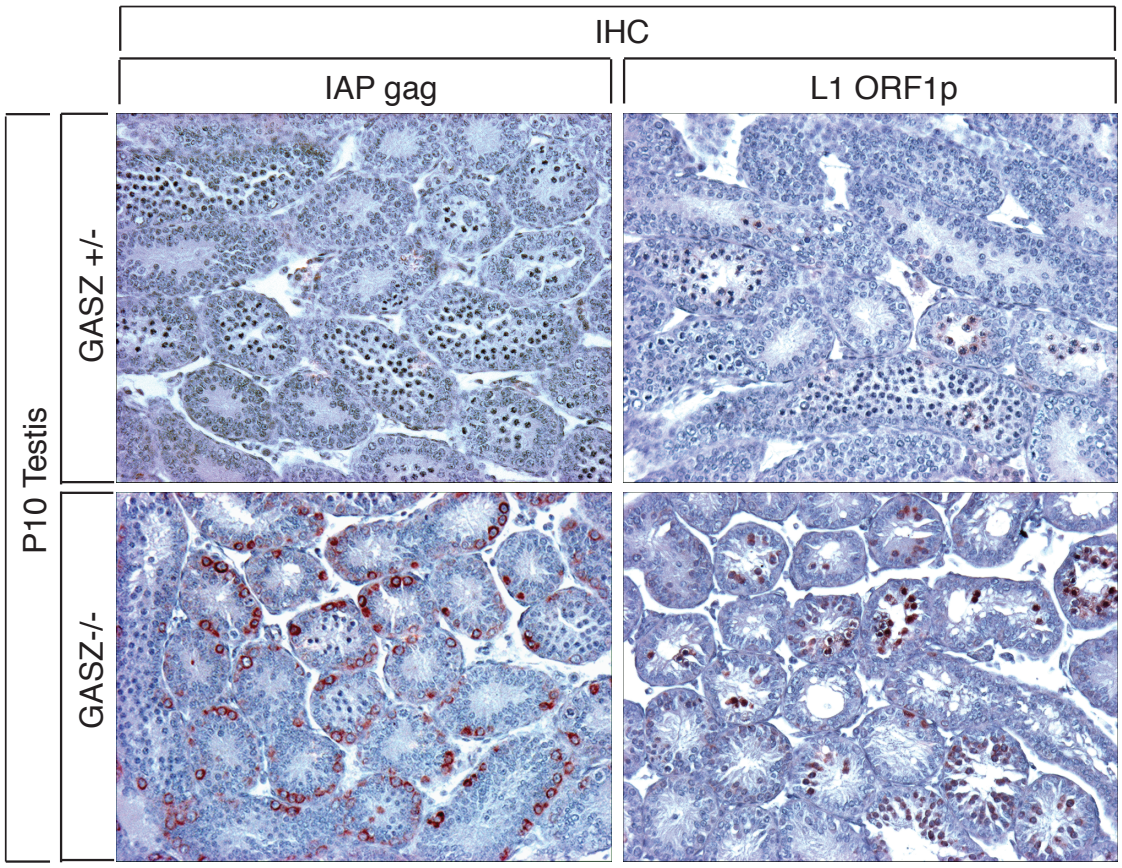

Supplemental 12. IAPgag and LINE-1 ORF1p expression in GASZ-/- mouse testis

Validation of the mouse IAP gag (Dewannieux, et al. 2004) and mouse LINE-1 ORF1p (Soper, et al. 2008) antibody by detecting expression (red) in mouse GASZ$^{-/-}$ testis. As previously reported in (Ma, et al. 2009) IAP gag and L1 ORF1p expression is readily detectable in GASZ$^{-/-}$ testis but absent in GASZ$^{+/-}$ of P10 testis.

Supplemental Table 6. Primer and Probe Sequences

RT-PCR primers were previously described in (Czech, et al. 2013; Link, et al. 2013; Vagin, et al. 2013). Stellaris FISH probes were designed as outlined in methods

Primer	Sequence
TAHRE Fwd	CTGTTGCACAAAGCCAAGAA
TAHRE Rev	GTTGGTAATGTTCGCGTCCT
Rp49 Fwd	ATGACCATCCGCCCAGCATACA
Rp49 Rev	CGTAACCGATGTTGGGCATCAGATACT
Idefix Fwd	AACAAAATCGTGGCAGGAAG
Idefix Rev	TCCATTTTTCGCGTTTACTG
Burdock Fwd	GCCATCCCAACAGCAAAATTC
Burdock Rev	TTTTGGCCCTGTAAACCTTG
HeT-A Fwd	TCCAACTTTGTAACTCCCAGC
HeT-A Rev	TTCTGGCTTTGGATTCCTCG
Gypsy Fwd	CCAGGTCGGGCTGTTATAGG
Gypsy Rev	GAACCGGTGTACTCAAGAGC
Flamenco Fwd1	CAGATTACCATTTGGCTATGAGGATCAGAC
Flamenco Rev1	TGGTGAAATACCAAAGTCTTGGGTCAA C
Flamenco Fwd 2	TCTGGAGGGTTTCCTCCTTT
Flamenco Rev 2	GGTGGTACGACCATCCAAAC
dp53_qPCR_Fwd	CTATTGAGCTGGCGTTCGTCTTGGAT
dp53_qPCR_Rev	TCTGCCAAAACTCGTGTATCGGGCG

DDPCR Primer/Probe Sequence

Primer/Probe	Sequence	Dye/Quencher
TAHRE Fwd	CTGTTGCACAAAGCCAAGAA	
TAHRE Rev	GTTGGTAATGTTCGCGTCCT	
TAHRE Probe	TCACCAGAGCAGTTGACGCAGG	Fam/Zen/IBFQ
Rp49 Fwd	ATGACCATCCGCCCAGCATACA	
Rp49 Rev	CGTAACCGATGTTGGGCATCAGATACT	

Rp49 Probe	ATCGATCCGACTGGTGGCGGATGAAGTG CTTGGT	HEX/ZEN/IBFQ

TAHRE Stellaris Probe Sequence (Quasar 570 Dye)

gtgttggtgagtatgtgaga
tttctgcgcttatgtttgtg
actagtaatggccttcttga
tattttcttggttgtgttcc
tgaccatgaagcgtagcaac
aaatgtctggctttgggttt
cactatttccagtacggttg
tcttttggtgggggaaatg
gcagaagggcataacgaagc
gctgctgataaattcacctc
ggctcctggaagatgaatta
aaactcataggctgctcttc
gggtgctattatatctggac
aaagctagagcagtccagat
taggagtcgcacgtaatctt
aaacgggtgtaatgagcggg
tctacatctgtgttctgagg
caatttccctcacattgttg
gactcctgctgtataattca
gattttgttgtaggcagtca
aaaggaaaaccgttggcggt
aggtgtctgatgatgactcg
cgagcatggtgtggaatgat
attcgtcatgtttctagcga
cttcaaacattcgcatgggg
gagataattttgccatggct
tgtttttcctttcgatatcc
catgaatttttggagtgcct

tgcaacaggatgacaggtga
ccttgtacgcactaatatgc
tttcagtcttataagcgggg
tccttgattgtccttatttt
tcgtccatagttggtaatgt
ggaaagttgttgcgagaggg
tgaggagctaaatggtagcc
cttgcttcgtttctgttttg
aaagtcgtgggaggagaagc
gccatttattcagacgtttc
tttggagacgttgtcagagt
aggattgctcgtcatgttag
agcttttcctggaacatttc
cctgatgtttgtcttctttt
ggatgttgtcgtctatgatc
ttttgcgggttagagtatgt
cttttgctgtcgaagtcaga
atattttccactcgttgtgt
gtagactctttcgtggattc
ttaggaggtcatgaggtgtg

ChIP Primer Sequences:

Primer Pair	LINE1 GFP Reporter ChIP	Forward	Reverse
1	5pUTR Minimal Promoter	GACGCAGAAGACGGTGATTT	TCACCCCTTTCTTTGACTCG
2	5pUTR Enhancer Region	CGCACCACGAGACTATATCC	CAGTCTGCCCGTTCTCAGAT
3	5pUTR Upstream Orf1	GGCACACTGACACCTCACAC	TAACAGACAGGACCCTCAGC
4	Orf1 Start	ACATCTACACCGAAAACCCATC	GCGCTCTGCGTTTTAGAGTT

Supplemental References

Coufal, N. G., et al.
2011 Ataxia telangiectasia mutated (ATM) modulates long interspersed element-1 (L1) retrotransposition in human neural stem cells. Proc Natl Acad Sci U S A 108(51):20382-7.

Czech, B., et al.
2013 A transcriptome-wide RNAi screen in the Drosophila ovary reveals factors of the germline piRNA pathway. Mol Cell 50(5):749-61.

Dewannieux, M., et al.
2004 Identification of autonomous IAP LTR retrotransposons mobile in mammalian cells. Nature genetics 36(5):534-9.

Ergun, S., et al.
2004 Cell type-specific expression of LINE-1 open reading frames 1 and 2 in fetal and adult human tissues. The Journal of biological chemistry 279(26):27753-63.

Giordano, J., et al.
2007 Evolutionary history of mammalian transposons determined by genome-wide defragmentation. PLoS Comput Biol 3(7):e137.

Haase, A. D., et al.
2010 Probing the initiation and effector phases of the somatic piRNA pathway in Drosophila. Genes Dev 24(22):2499-504.

Khan, H., A. Smit, and S. Boissinot
2006 Molecular evolution and tempo of amplification of human LINE-1 retrotransposons since the origin of primates. Genome Res 16(1):78-87.

Kirino, Y., et al.
2010 Arginine methylation of Aubergine mediates Tudor binding and germ plasm localization. RNA 16(1):70-8.

Klattenhoff, C., et al.
2009 The Drosophila HP1 homolog Rhino is required for transposon silencing and piRNA production by dual-strand clusters. Cell 138(6):1137-49.

Link, N., et al.
2013 A p53 enhancer region regulates target genes through chromatin conformations in cis and in trans. Genes Dev 27(22):2433-8.

Ma, L., et al.
2009 GASZ is essential for male meiosis and suppression of retrotransposon expression in the male germline. PLoS Genet 5(9):e1000635.

Nishida, K. M., et al.
2007 Gene silencing mechanisms mediated by Aubergine piRNA complexes in Drosophila male gonad. RNA 13(11):1911-22.

Petitjean, A., et al.
2007 Impact of mutant p53 functional properties on TP53 mutation patterns and tumor phenotype: lessons from recent developments in the IARC TP53 database. Human mutation 28(6):622-9.

Rakheja, D., et al.
2014 Somatic mutations in DROSHA and DICER1 impair microRNA biogenesis through distinct mechanisms in Wilms tumours. Nat Commun 2:4802.

Rodic, N., et al.
2014 Long interspersed element-1 protein expression is a hallmark of many human cancers. Am J Pathol 184(5):1280-6.

Saito, K., et al.
2010 Roles for the Yb body components Armitage and Yb in primary piRNA biogenesis in Drosophila. Genes Dev 24(22):2493-8.
Soper, S. F., et al.
2008 Mouse maelstrom, a component of nuage, is essential for spermatogenesis and transposon repression in meiosis. Dev Cell 15(2):285-97.
Vagin, V. V., et al.
2013 Minotaur is critical for primary piRNA biogenesis. RNA 19(8):1064-77.